

Short Communication

## Investigation of Effect of Heat Treatment on the Han Dynasty Steel Sword Corrosion by Electrochemical Corrosion Testing

Wei Wu<sup>1,2</sup>, Xiaocen Li<sup>1,\*</sup>

<sup>1</sup> Cultural Heritage Protection and Scientific Cognition Research Base, Nanjing University of Information Science and Technology, Nanjing Jiangsu Province 210044, China.

<sup>2</sup> School of Materials Engineering, North China Institute of Aerospace Engineering, Langfang Hebei Province 065000, China.

\*E-mail: [wuwei3873@163.com](mailto:wuwei3873@163.com); [lixiaocenp@163.com](mailto:lixiaocenp@163.com)

Received: 11 October 2022 / Accepted: 16 November 2022 / Published: 27 December 2022

---

Different quenching treatments with two heating temperatures (820 °C and 940 °C) were carried out in several quenching medium (mineral water, vinegar, and pig grease) on modern Chinese swords to simulate the ancient quenching process prevalent during the Han dynasty. The electrochemical corrosion behavior of these swords in the soil from the Han dynasty buried layer were measured in an attempt to discern the method of heat treatment of an ancient steel sword found in the same layer of earth. The results show that the corrosion resistance of the test swords in the soil increased with decreasing quenching temperature. Furthermore, the sword heated at 820 °C and quenched with mineral water showed the lowest corrosion rate in the Han dynasty buried soil. However, the sample heated at 940 °C and quenched with mineral water showed the most similar electrochemical behavior to the ancient sword. Therefore, we speculate that the ancient sword was also heat treated in this manner.

---

**Keywords:** A. Steel sword; B. Quenching; C. Corrosion; D. Electrochemical test

### 1. INTRODUCTION

As an advanced cold weapon in ancient times, the steel sword not only played a vital role in war, but also presently has scientific and technological value to the study of the history of the iron industry. In order to achieve the most desirable combination of strength and toughness in a sword, many ancient craftsmen from Japan, China, Indonesia, Persia, India, and several European countries frequently forged two or more pieces of steel with different carbon content into one sword with a laminated structure [1]. Typical ancient Chinese swords were made of medium (or high) carbon steel sandwiched by two pieces of low carbon steel or wrought iron and showed duplex construction, as

shown in Figure 1. Medium or high carbon levels provide strength and hardness in a sword, while low carbon steel provides toughness. The quality of strength and hardness can be further enhanced by a quenching process. Water, vinegar, urine, and animal grease were all used as quenchant according to the literature [2]. Obviously, these different types of cooling medium have different effects on the quenching process and thus affect the mechanical and corrosion properties of swords.

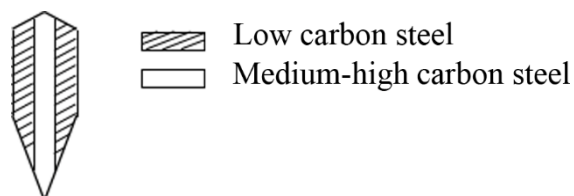


**Figure 1.** Cross-sectional structure of a Chinese sword with duplex construction

Since iron and steel swords are easily corroded, they are not well preserved in fossil soil, and thus few ancient swords have been unearthed. The environment, raw materials, and heat treatment process all have important effects on the corrosion and preservation of swords buried in soil. The question of how the ancient swords were molded and heat treated is difficult to determine. The details about the quenching which is the most important step in the heat-treatment of a sword still puzzles researchers. Some physical methods such as neutron diffraction, scanning electron microscopy, energy dispersive X-ray spectroscopy, energy dispersive X-ray fluorescence spectrometry, differential scanning calorimetry, and Vickers micro-hardness test are usually used to characterize the microstructure of ancient swords and drive speculate their technique [3-11].

However, few studies have examined the possible heat treatment of an ancient sword through the sword's electrochemical corrosion behavior and preservation status of such sword or its remnants relics in the buried soil environment where it was unearthed. In this study, several artificial swords that have the same chemical composition to a Han dynasty sword were forged and heated at two different temperatures then quenched with different medium. The electrochemical corrosion behavior of these artificial swords and a real Han dynasty sword found in buried soil were then measured and compared by electrochemical measurements in an attempt to determine the possible quenching process.

## 2. EXPERIMENTAL METHODS

### 2.1 Sample preparation

The samples in this study were divided into two categories, one category was taken from the artificial swords forged with medium carbon steel and low carbon steel, and another was taken from the excavated Han dynasty sword. The chemical constitution of the medium and low carbon steels used on the artificial swords was exactly the same as the Han dynasty sword, as shown in Table 1.

**Table 1.** Composition of the steel samples (wt.%)

C	Si	Mn	P	S
0.5	0.05	0.15	0.03	0.02

Three cooling medium (mineral water, vinegar, and pig grease), which were recorded in the literature were used in this study [2]. As ancient craftsmen quenched according to experience and could not measure and control the temperature precisely, two temperatures of 940 °C and 820 °C were adopted that correspond to austenitizing and sub-austenitizing, respectively [12-13]. The samples heated at 940 °C and 820 °C and quenched with mineral water, vinegar, and pig grease were named as 940-w, 940-v, 940-g, 820-w, 820-v, and 820-g, respectively. Two samples were cut from the Han dynasty sword and named as sd-1 and sd-2. These samples were cut into cuboids of 10×5×5mm along the longitudinal section of the sword and were ground by emery cloth from 320 to 2000 grit, subsequently polished with 100 nm diamond spray suspension, and then cleaned thoroughly with deionized water and alcohol in turn.

## 2.2 Electrochemical tests

In order to explore the corrosion of the ancient sword and try to infer how it was quenched, electrochemical tests were performed on the above eight samples using an electrochemical workstation (CORRTEST CS350H). Electrochemical corrosion tests were performed in water-saturated soil, and the soil came from the same location where the Han dynasty sword was buried. The soluble salt content of soil was summarized in Table 2. A three-electrode system was used with a platinum sheet as the auxiliary electrode and a saturated calomel electrode (SCE) as the reference electrode. Potentiodynamic polarization measurements were carried out at 250 mV below the open circuit potential (OCP) and scanned toward the positive direction with a scan rate of 1 mV/s until the anodic current density reached 1mA/cm<sup>2</sup>. Tafel extrapolation was used to analyze the polarization curves, and an electrochemical impedance spectrum (EIS) test was carried out at the OCP under a 10 mV AC excitation voltage with a frequency range of 0.01 Hz to 100 kHz [14-17].

**Table 2.** Composition of soil (mg/kg)

Ca <sup>2+</sup>	Na <sup>+</sup>	Mg <sup>2+</sup>	K <sup>+</sup>	Cl <sup>-</sup>	SO <sup>2-</sup>	NO <sup>3-</sup>
405.23	332.56	156.32	69.29	Cl <sup>-</sup>	1426.48	106.35

## 2.3 Microstructure and microhardness measurement

Observations of metallographic and corrosion morphology were provided by optical microscope and scanning electron microscope (SEM). The hardness of the samples quenched with different medium was measured with a Vickers hardness tester.

### 3. RESULTS AND DISCUSSION

#### 3.1 Microstructure and microhardness measurement

Typical metallographic features of quenched samples obtained by optical microscope are shown in Figure 2, where Figures 2 a–h correspond to 940-w, 940-v, 940-g, 820-w, 820-v, 820-g, sd-1, and sd-2, respectively.

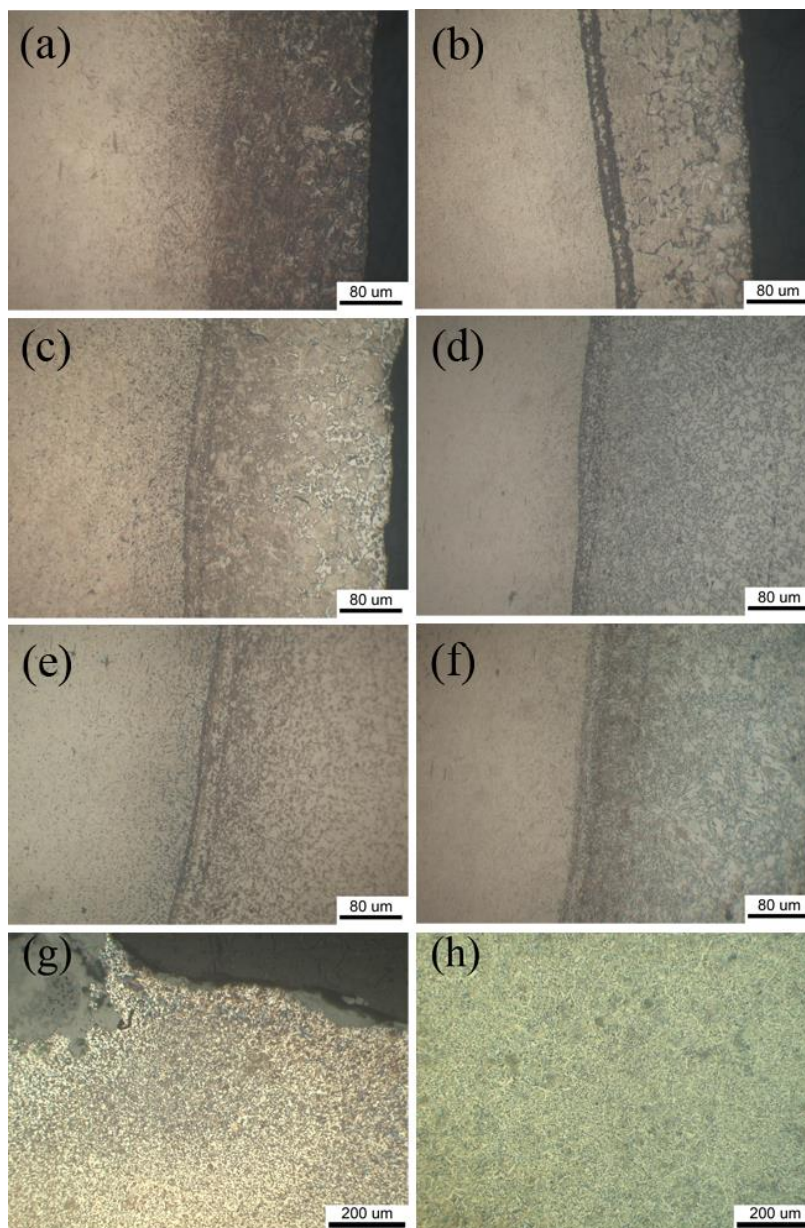


**Figure 2.** Typical metallographic morphologies of swords with different quenching conditions, (a) 940-w, (b) 940-v, (c) 940-g, (d) 820-w, (e) 820-v, (f) 820-g, (g) sd-1, (h) sd-2

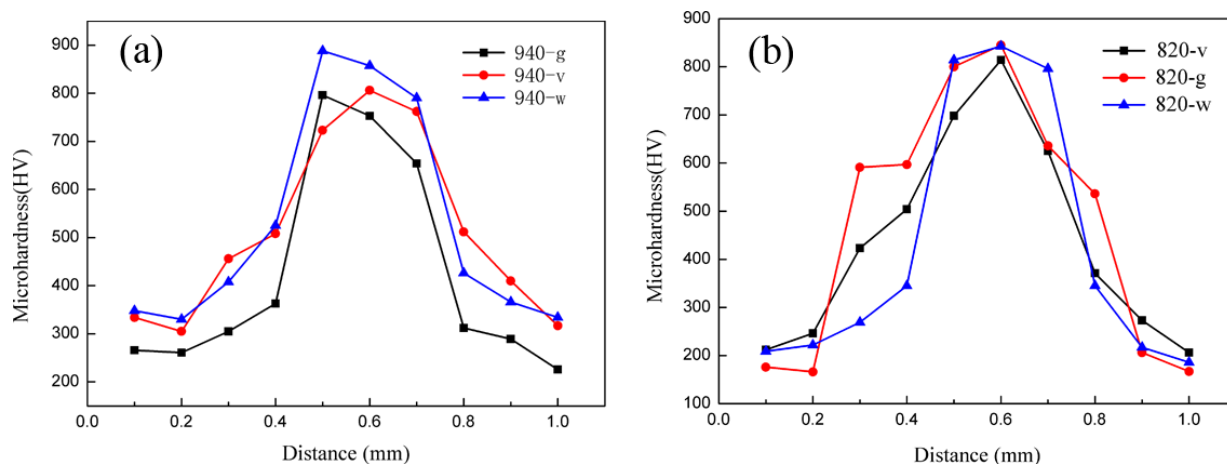


**Figure 3.** (a) The microhardness curve of 940 °C quenching, (b) The microhardness curve of 820 °C quenching

The cooling rate of a quenched sword is greatest in mineral water, followed by vinegar, then pig grease [18]. At 940 °C, the microstructures varied from ferrite and pearlite to lath martensite on both sides in different cooling medium, and the structure in the core was completely transformed to acicular martensite. In contrast, the microstructures on both sides were only ferrite and pearlite at a temperature of 820 °C. In general, a higher temperature usually promotes martensitic transformation of low-carbon steel. In addition, the medium-carbon microstructure was more easily transformed into martensite compared to the low-carbon microstructure with a fast cooling rate.

The hardness of quenched duplex construction on the outsides was lower than that in the core. The 940-w had the highest hardness value (888HV) in the core, and the hardness value on its outsides (350HV) was still higher than others, as shown in Figure 3(a). Compared to the above quenching conditions, pig grease quenching (820-g) showed the best comprehensive properties because it had the hardest core (845HV) and the softest outsides (166HV), as shown in Figure 3(b).

The metallographic structure of the Han dynasty sword was clean and without large inclusions, as shown in Figure 2(g), (h). The blade was pearlite and ferrite with equiaxial grains, but the amount pearlite on outsides of the edge increased significantly due to carburization, as shown in Figure 2(g). It was difficult to evaluate quantitatively the microstructure differences from just the optical microscope, and thus it was difficult to speculate on the craftsmanship of the ancient sword. However, electrochemical response can reflect obvious differences in microstructure.

### 3.2 Potentiodynamic polarization tests

The potentiodynamic polarization curves of the eight samples as measured in the Han dynasty soil environment after OCP stabilization are shown in Figure 4. The polarization curves of the eight samples were similar in shape indicating that all the samples had experienced the same corrosion reactions.

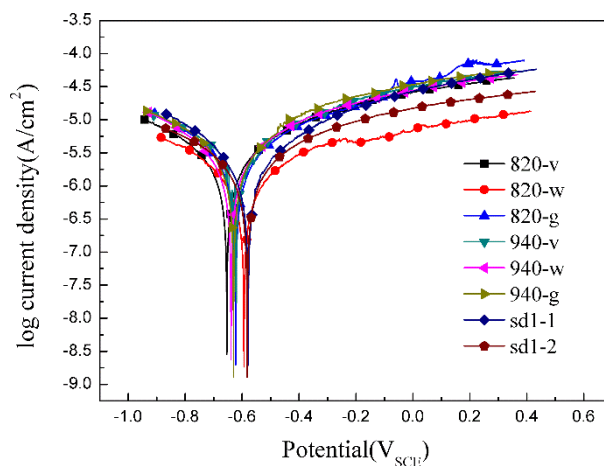


**Figure 4.** Potentiodynamic polarization curves of the samples in water-saturated soil

The anodic current density increased significantly when the polarization potential exceeded  $E_{\text{corr}}$ , which indicates that the active dissolution of the metal directly affected and controlled the anodic branch. The cathodic branch also had a similar shape, indicating that the cathodic reaction followed a common corrosion law. That is, the oxygen reduction reaction was not affected by the changing quenching temperatures and cooling medium. When the applied overpotential was above 110 mV at the anodic branch and above 85 mV at the cathodic branch relative to the corrosion potential  $E_{\text{corr}}$ , the log current density was approximately linear with the applied potential and approached Tafel-type behavior [17, 19-21]. The polarization curve was fitted by Tafel extrapolation, and the relevant results are shown in Table 3.

The anodic Tafel slope ( $b_a$ ) shows the resistance of the anode reaction, which in this case was the ionization of iron. The cathodic Tafel slope ( $b_c$ ) indicates the resistance of oxygen reduction, which was the resistance of oxygen to hydroxide [22-24]. If the corrosive power is ignored, a larger corrosion resistance corresponds to a slower corrosion rate. The high  $b_a$  values reveal that the resistance of iron dissolution was large and that the soil environment was not overly corrosive to the samples, a fact that was helped by poor diffusion conditions in soil. Correspondingly, the diffusion rate of oxygen was also reduced, resulting in an increase in  $b_c$  values. Importantly, since the corrosion rate is the result of the combined effect of the corrosion resistance of the swords and the corrosive ability of soil,  $i_{\text{corr}}$  can actually comprehensively reflect the corrosion rate [24-26].

As shown in Table 3, at 820 °C and 940 °C, the samples quenched with mineral water had the smallest  $i_{\text{corr}}$ , and the samples quenched with pig grease had the largest. The vinegar-quenched samples had the in-between  $i_{\text{corr}}$ , indicating that the corrosion rate increased as the cooling rate decreased during quenching. For a given cooling medium, the  $i_{\text{corr}}$  value of 820 °C was lower than that of 940 °C, indicating that the samples quenched at 820 °C had better corrosion resistance. In addition, the  $i_{\text{corr}}$  of the Han dynasty sword was between 1.1 and 1.2  $\mu\text{A}\cdot\text{cm}^{-2}$ , which is very close to the value of 940-w, and we presumed that the sword would have been put through water quenching at this temperature. Although our Tafel fitting analysis was subjective [27], we believe the results used in comparing the effect of different quenching conditions on corrosion are reasonable since the mean and standard deviation of repeated tests were within a reasonable range.

**Table 3.** Tafel extrapolation results for potentiodynamic polarization curves of samples

Samples	$b_a$ (mV·dec <sup>-1</sup> )	$b_c$ (mV·dec <sup>-1</sup> )	$i_{corr}$ (μA·cm <sup>-2</sup> )	Corrosion Rate (μm/A)
820-w	349±41	203±26	0.71296±0.07	8.3639±0.8
820-v	343±41	235±30	1.5705±0.18	18.424±2.21
820-g	336±40	277±36	1.6855±0.21	19.773±2.37
940-w	286±34	280±36	1.4606±0.17	18.307±2.19
940-v	261±31	292±38	1.6789±0.22	19.696±2.56
940-g	256±30	306±39	2.9928±0.38	35.109±4.56
sd-1	276±33	181±23	1.2848±0.16	15.072±1.95
sd-2	289±34	206±26	1.0811±0.14	12.682±1.64

### 3.3 EIS measurements

EIS measurements were used to evaluate the corrosion kinetics of the eight samples under the different quenching conditions. The Nyquist plots (Fig. 5) show similar depressed arc features. All of the tested samples presented one obvious capacitive arc at high and middle frequency ranges [28-29]. Apparently, the radius of the Nyquist loop increased significantly with increasing cooling rate during quenching, indicating a better corrosion resistance for the sample quenched with mineral water. In addition, all of the samples exhibited relatively large ohmic resistance (10<sup>4</sup> Ω) as a result of the accumulation of corrosion products on the metal surfaces and restricted oxygen diffusion in the soil. In such an environment the charge transfer resistance and film ohmic resistance usually exhibit large values.

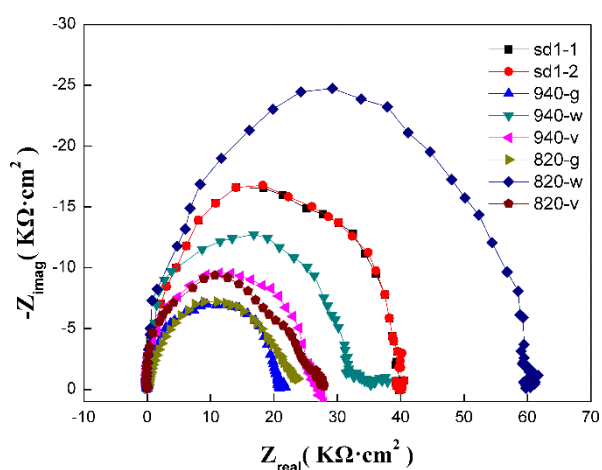


**Figure 5.** Typical Nyquist plots of EIS tests of the samples

In order to analyze corrosion kinetics under different quenching conditions quantitatively, the equivalent electrical circuit shown in Figure 6 was used to fit the Nyquist spectra because of its error of fit ( $\chi^2 < 1 \times 10^{-3}$ ). The elements of the equivalent circuit are defined as follows:  $R_s$  is soil resistance,  $Q_{hf}$  is the constant phase element (CPE) associated with the interface capacitance at high frequency,

$R_{po}$  represents the resistance of wet soil and corrosion products,  $R_{ct}$  is the charge transfer resistance at the active corroded surface, and  $Q_{lf}$  is the interfacial capacitance of the corroded surface at low frequencies [30-32].

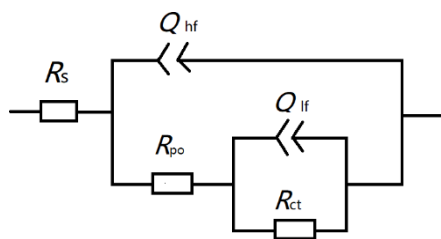


**Figure 6.** The equivalent circuit used to fit the EIS tests

Table 4 shows the fitted values of  $R_f$  and  $R_{ct}$  in the equivalent electrical circuit. Both  $R_f$  and  $R_{ct}$  increased with the quenching cooling rate, indicating that water quenching had the largest resistance to active dissolution (slowest corrosion rate). Since water quenching produced more martensite than pig grease quenching, we may infer that the corrosion resistance was related to the amount of martensite. However, for a given cooling medium, the  $R_f$  and  $R_{ct}$  values at 940 °C were smaller than that at 820 °C, indicating that the corrosion resistance of the samples quenched at 940 °C was smaller even though high temperature quenching produced more martensite.

Martensite usually contains more dislocation and higher residual stress that usually promote the propagation of corrosion. The regularity of the  $R_f$  values further indicated that its acicular martensite had a significant effect on corrosion resistance. Additionally, the  $R_f$  and  $R_{ct}$  values of the Han dynasty sword samples were very close to the corresponding values of 940 °C water quenching. Therefore, we speculate that the ancient sword was quenched under these conditions, which is consistent with the conjecture we obtained from our Tafel fitting results of the potentiodynamic polarization curves.

**Table 4.** The fitting results of the EIS experimental data

Samples	$R_{hf} (\Omega \cdot \text{cm}^2)$	$R_{ct} (\Omega \cdot \text{cm}^2)$
820-w	13996±1679	46565±5587
820-v	13825±1659	13644±1637
820-g	11399±1367	11086±1330
940-w	13075±1569	23774±2852
940-v	12460±1370	12767±1404
940-g	11250±1237	9655±1062
sd-1	13767±1514	23284±2561
sd-2	12899±1418	24005±2640

### 3.4 Corrosion morphologies

Figure 7 shows the SEM images of samples under different quenching conditions. The corrosion of the low-carbon structures on the outside was more severe than that of the medium-carbon structures in the core, especially for samples quenched at 940 °C. This was primarily due to lath martensite with coarse grains and increased retained austenite at higher temperature. The sample quenched with pig grease had the worst corrosion resistance because of its slower cooling rate resulting in C-curve shift and faster diffusion of carbon. Thus, all factors that contributed to inhomogeneous microstructure were the main reasons for severe corrosion. In addition, the distribution of corrosion products on the Han dynasty sword sample was relatively dense, and the appearance of micro-cracks that are usually generated in a higher quench temperature further supported our speculation about the ancient sword's quenching process, as shown in Figure7(g), (i): its corrosion was close to that of the water quenched samples at 940 ° C.

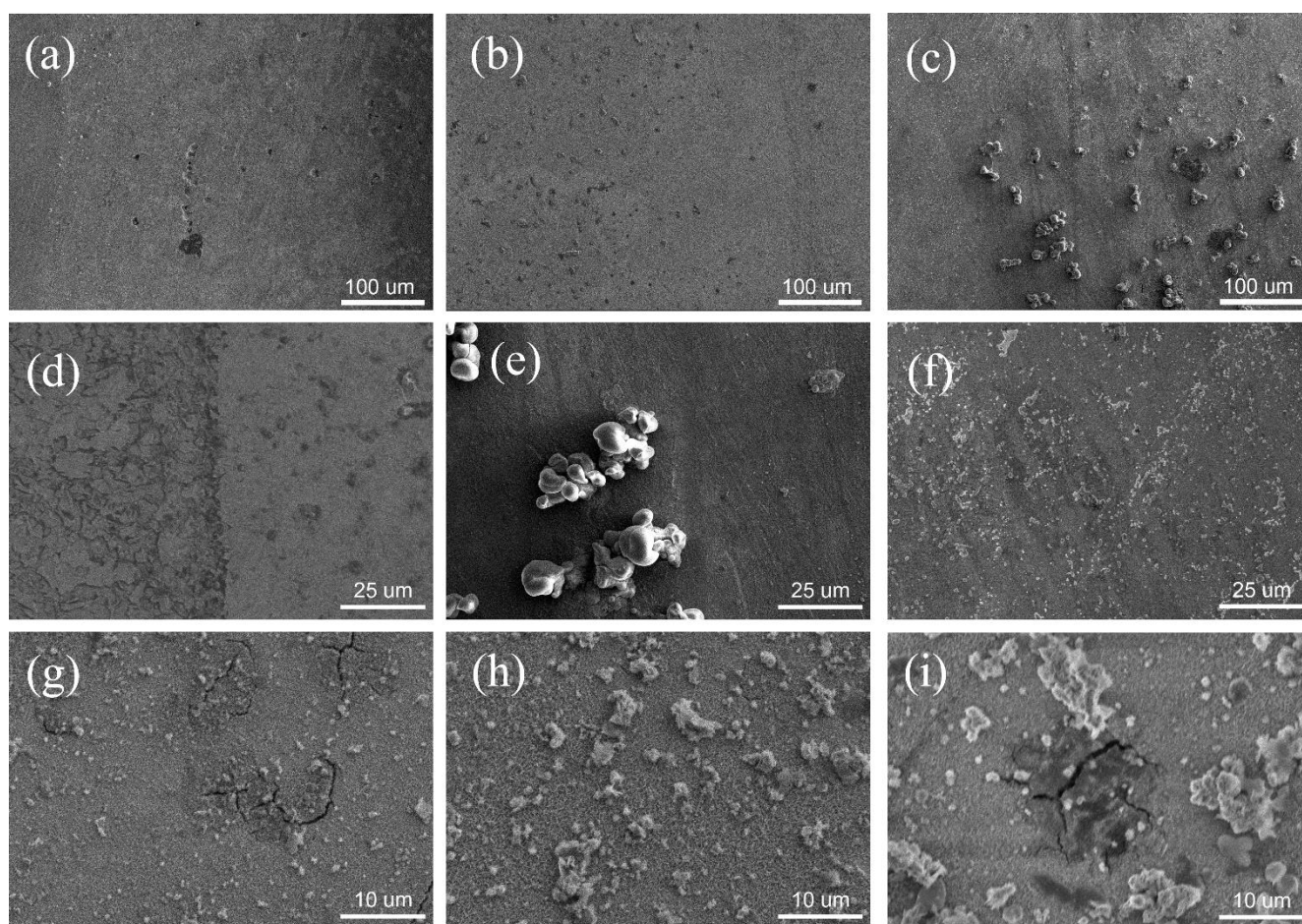


**Figure 7.** Typical corrosion morphologies of the samples, (a) 820-w, (b) 820-v, (c) 820-g, (d) 940-w, (e) 940-v, (f) 940-g, (g) sd-1, (h) sd-2, (i) sd-1

## 4. CONCLUSIONS

The microstructure, hardness, and corrosion resistance of artificial steel swords quenched at different temperatures with different cooling medium were measured in an effort to determine the

quench technique used on an ancient Han dynasty sword that had evidently been processed by carburizing and quench. Our conclusions are enumerated below.

(1) Pig grease was the best cooling medium for a sword to achieve the ideal combination of strength and toughness. The outsides of the sword quenched in this manner contained more pearlite than its core part.

(2) Potentiodynamic polarization curves showed that the corrosion resistance of the swords was improved by increasing the cooling rate. The sword quenched with water had the best corrosion resistance, and the swords quenched at 820 °C had better corrosion resistance than those quenched at 940 °C. The  $i_{\text{corr}}$  value of the Han dynasty sword was most similar to the value of the 940-w sample. Therefore, we speculate that the ancient sword was heated at 940 °C and quenched with mineral water.

(3) The diameter of Nyquist plots increased with the cooling rate, and showed larger values at lower heating temperatures (820 °C). The samples heated at 820 °C and quenched with water had the biggest film ohmic and charge transfer resistance, and the value of  $R_f$  and  $R_{ct}$  for the Han dynasty sword was very similar to that of 940-w, indicating that the ancient Han dynasty sword may have experienced a similar quenching process.

(4) Corrosion morphology also showed that the 820-w sample exhibited the smallest corrosion intensity. The Han dynasty sword showed an analogous corrosion morphology to 940-w, and it may have experienced the same quench process.

#### ACKNOWLEDGEMENTS

This research was sponsored by the National Natural Science Foundation of China under Grant No. 51861135307, the Postgraduate Scientific Innovation Research of Jiangsu Province under Grant No. KYCX21\_0981, the Science and Technology Support from Langfang city under Grant No. 2022011034, 2021011076, and Scientific Research of Universities of Hebei Province under Grant No. ZC2022025.

#### References

1. J. Wadsworth, *Mater. Charact.*, 99 (2015) 1.
2. J. Needham, *Science and Civilization in China*, Cambridge University Press, (2008), Cambridge, United Kingdom.
3. J. S. Park, K. Rajan, and R. Ramesh, *Archaeometry*, 62 (2020) 68.
4. F. Salvemini, A. Williams, D. Edge, B. Schillinger, F. Cantini, and F. Grazzi, *Microchem. J.*, 159 (2020) 105397.
5. F. Y. Zhao, M. Sun, X. H. Li, F. Guo, and M. Y. Li, *SN Appl. Sci.*, 2 (2020) 1510.
6. Y. Salem, O. Oudbashi, and D. Eid, *Herit. Sci.*, 7 (2020) 19.
7. S. Harjo, T. Kawasaki, F. Grazzi, T. Shinohara, and M. Tanaka, *Materialia*, 7 (2019) 100377.
8. K. Shizuma, T. Kajimoto, S. Endo, K. Matsugi, Y. Arimatsu, and H. Nojima, *Nucl. Instrum. Meth. B*, 407 (2017) 244.
9. G. Dini, *JOM*, 70 (2018) 243.
10. G. Ghiara, *JOM*, 66 (2014) 793.
11. P. Fajfar, J. Medved, G. Klančnik, T. Lazar, M. Nečemer, and P. Mrvar, *Mater. Charact.*, 86 (2013) 232.

12. Q. Y. Qin, J. Xu, B. X. Wei, Q. Fu, C. K. Yu, C. Sun, and Z. Y. Wang, *Corros. Sci.*, 200 (2020) 110228.
13. Y. Liang, Y. X. Du, L. Chen, N. P. Tian, L. Zhang, and L. J. Qiao, *Eng. Fail. Anal.*, 135 (2022) 106112.
14. W. M. Tian, F. F. Chen, F. S. Cheng, Z. L. Li, and G. X. Pang, *Int. J. Electrochem. Sci.*, 15 (2020) 9120.
15. Z. P. Liang, K. X. Jiang, B. A. Feng, S. N. Lin, X. Chao, Q. Q. Sui, and T. A. Zhang, *J. Electroanal. Chem.*, 899 (2021) 115688.
16. Q. Wang, X. M. Cao, T. Q. Wu, M. Liu, C. Li, and F. C. Yin, *Int. J. Pres. Ves. Pip.*, 194 (2021) 104508.
17. W. M. Tian, Z. L. Li, H. F. Kang, F. S. Cheng, F. F. Chen, and G. X. Pang, *Materials*, 13 (2020) 3236.
18. H. Watanabe, *J. Chem. Eng. Data*, 48 (2003) 124.
19. W. M. Tian, F. F. Chen, Z. L. Li, G. X. Pang, and Y. B. Meng, *Corros. Sci.*, 173 (2020) 108775.
20. K. M. Jafery, Z. Embong, N. K. Othman, N. Yaakob, M. Shah, and N. Z. N. Hashim, *Mater. Today: Proceedings*, 51 (2022) 1381.
21. Q. Y. Qin, B. X. Wei, Y. L. Bai, Q. Fu, J. Xu, C. Sun, C. Wang, and Z. Y. Wang, *Eng. Fail. Anal.*, 120 (2021) 105065.
22. B. X. Wei, J. Xu, Y. F. Cheng, C. Sun, C. K. Yu, and Z. Y. Wang, *Corros. Sci.*, 193 (2021) 109893.
23. M. Zhu, B. Z. Zhao, Y. F. Yuan, S. M. Yin, S. Y. Guo, and G. Y. Wei, *Mater. Chem. Phys.*, 279 (2022) 125725.
24. W. M. Tian, F. F. Chen, Z. L. Li, G. X. Pang, and Y. X. Li, *Int. J. Electrochem. Sci.*, 15 (2020) 6572.
25. L. Kang, Q. Zeng, B. Wang, J. S. Zeng, B. K. Liao, H. X. Wu, Z. Cheng, and X. P. Guo, *Sep. Purif. Technol.*, 284 (2022) 120266.
26. R. M. Azoor, R. N. Deo, N. Birbilis, and J. Kodikara, *Corros. Sci.*, 159 (2019) 108116.
27. S. Rossi, M. Pinamonti, and M. Calovi, *Case Stud. Constr. Mat.*, 17 (2022) e01257.
28. X. B. Zhou, Z. F. Zhou, T. Q. Wu, C. Li, and Z. Li, *Corrosion Communications*, 3 (2021) 23.
29. M. Zhu, B. Z. Zhao, Y. F. Yuan, S. Y. Guo, and G. Y. Wei, *J. Electroanal. Chem.* 882 (2021) 115026.
30. H. W. Liu, Y. F. Cheng, *J. Mater. Res. Technol.*, 9 (2020) 7180.
31. H. C. Ma, B. Zhao, Z. Y. Liu, C. W. Du, and B. N. Shou, *Constr. Build. Mater.*, 243 (2020) 118203.
32. Y. X. Fan, C. Y. Chen, Y. X. Zhang, H. X. Liu, H. W. Liu, and H. F. Liu, *Bioelectrochemistry*, 141 (2021) 107880.